Microsystem Technologies (2022) 28:269–274
https://doi.org/10.1007/s00542-019-04687-7

TECHNICAL PAPER

Comparative study of PTB7:$PC_{71}BM$ based polymer solar cells fabricated under different working environments

Ram Datt[1,2] · Sandeep Arya[3] · Swati Bishnoi[1] · Ramashanker Gupta[1,2] · Vinay Gupta[4] · Ajit Khosla[5]

Received: 31 October 2019 / Accepted: 6 November 2019 / Published online: 14 November 2019

Abstract

In this article, we have evaluated the performance of inverted organic solar cells (OSCs) fabricated under ambient air and inert environment. Here, poly([4,8-bis[(2-ethylhexyl)oxy]benzo[1,2-b:4,5-b′]dithiophene-2,6-diyl]{3-fluoro-2-[(2-ethylhexyl)carbonyl]thieno[3,4-b]thiophenediyl}) (PTB7) donor with [6,6]-phenyl C70-butyric acid methyl ester ($PC_{71}BM$) acceptor were employed as a photoactive layer. The calculated power conversion efficiency (PCE) from current–voltage (J–V) characteristics for a device fabricated under an inert environment is 6.90% as compared to 3.96% for a device fabricated in ambient condition (25 °C, 100 kPa). The results revealed that the device processed in ambient conditions degrades the photovoltaic performance parameters, and the PCE decreased by 42.62% as compared to the devices fabricated in an inert environment. Along with this, we have also discussed in detail, the effect of the working environment on photoactive layers by Raman spectroscopy. The UV–Vis spectroscopy and Atomic Force Microscopy (AFM) techniques are presented to illustrate the optical properties and morphology of the photo-active layer respectively.

1 Introduction

The development of organic solar cells (OSCs) received tremendous attention in recent years due to several advantages like; use of non-toxic and flexible materials, lightweight, environmentally friendly, and solution-processed roll to roll processing (Brabec 2004; Balderrama et al. 2013; Gupta et al. 2016; Zhao et al. 2017; Wang et al. 2014, 2017). Recently, researchers have achieved PCE over 13% (Zhao et al. 2017; Xu et al. 2018) in single junction OSCs using novel and efficient donor–acceptor materials as an active blend layer. The roll to roll fabrication process is the most dominant one for large scale fabrication of OSCs (Zhang et al. 2016). However, the complete fabrication process is still challenging to realize in an inert environment. Moreover, it is also known that OSCs degrade in ambient conditions due to the low environmental stability of organic semiconductor materials (Balderrama et al. 2016). As per literature, the almost all OSCs devices fabrication process reported, in an inert environment. However, the effect of fabrication processes carried under an ambient-air condition is not commonly reported. Therefore, a more detailed analysis is required to know the consequences of the fabrication process, under ambient conditions.

Here, we reported the performance of inverted PTB7:$PC_{71}BM$ OSCs fabricated under three different environmental conditions. In the first case study, fabricated one reference device in a nitrogen environment, and other two test devices in an ambient conditions with slight variation in their fabrication process as mentioned in the device fabrication section. The device fabrication process

✉ Sandeep Arya
snp09arya@gmail.com

Vinay Gupta
drvinaygupta@netscape.net

1 Advanced Materials and Devices Division, CSIR-National Physical Laboratory, Dr. K. S. Krishnan Marg, New Delhi 110012, India

2 Academy of Scientific and Innovative Research (AcSIR), Ghaziabad 201002, India

3 Department of Physics, University of Jammu, Jammu, Jammu and Kashmir 180006, India

4 Department of Mechanical and Materials Engineering, Masdar Institute, Khalifa University of Science and Technology, P.O. Box 54224, Masdar City, Abu Dhabi, United Arab Emirates

5 Department of Mechanical Systems Engineering, Faculty of Engineering, Yamagata University, Yonezawa, Yamagata 992-8510, Japan

in ambient conditions include steps like solvent and blend preparation, active layer spin coating and annealing process. The absorption, structural, and morphological analysis of all the three batch photoactive layer films were analyzed to perceive the role of environmental conditions on their properties. The significance of this study is to help in the design, fabrication, and optimization of the OSCs in ambient-air conditions and to reduce the overall practical efforts of device fabrication at a large scale.

2 Experimental details

2.1 Materials

Indium tin oxide (ITO) coated glass substrates were purchased from Latech, Singapore having sheet resistance 15–20 O/sq. The donor PTB7 and accepter $PC_{71}BM$ used in fabricating devices were purchased from 1-Material, Canada. Molybdenum (VI) oxide (99.999% purity) and Zinc acetate were purchased from Alfa Aesar, USA and Sigma-Aldrich, respectively.

2.2 Measurements and characterization

SCIENCETECH FS-02 solar simulator were used to measure photovoltaic characteristics of fabricated devices. The Keithley 2420 unit was used as source meter. The measurements conducted under exposure of AM 1.5 with the intensity of 100 mW/cm^2. The nanomorphology of PTB7:$PC_{71}BM$ bulk heterojunction (BHJ) films were examined by Veeco Nano Scope V atomic force microscopy (AFM). The absorption spectra was recorded by UV 2401PC, Shimadzu UV–Vis spectroscopy. The Raman spectroscopy was performed by HORIBA T64000 at Source wavelength of 514 nm.

The glass substrates were used to prepared sample films UV–Vis spectroscopy and AFM at same procedure and condition as prepared for device fabrication.

2.3 Device fabrication

Three different groups of OSCs were fabricated under different environmental conditions. Fabricated devices were categorized in A, B, and C batches. Batch A devices were fabricated completely inside glovebox (N_2 filled) used as a reference. Whereas B and C batches devices are fabricated in ambient-air (18 °C temperature, 69% relative humidity) conditions. The photoactive layer annealing environment is different for batch B (in vacuum oven, 29 mbar) and C (in ambient condition) devices.

The complete fabrication process step by step is shown in Fig. 1. ITO substrates patterned by laser scriber and cleaned by wet chemical method with deionized water followed by acetone, and isopropanol. Cleaned substrates dried in oven and UV-O_3 treated for 15 min before use. PTB7 and $PC_{71}BM$ used to prepared blend (25 mg/ml) 1:1.5 (w/w%), dissolved in chlorobenzene (CB) with 1,8-diiodooctane (DIO) 3% (v/v%). Zinc oxide (ZnO) prepared via a sol–gel process by using 0.1 M concentration of zinc acetate dehydrate [Zn(CH3COO)·2H_2O] in anhydrous ethanol, and added ethanolamine to the solution.

The fabricated device structure is ITO/ZnO/photoactive layer/MoO_3/Al (Fig. 2a), and Fig. 2b are shown the energy levels (eV) diagrams. The ZnO was spin casted over precleaned ITO substrates at 3000 rpm for 45 s and baked at 200 °C for 2 h. The blend solution was spin casted over ZnO film at 1000 rpm for the 60 s and annealed at 80 °C for 10 min to remove residue solvent. The MoO_3 ($\sim$ 10 nm) layer was thermally deposited followed by Al ($\sim$ 100 nm) in high vacuum ($\sim 4 \times 10^{-6}$ mbar) by thermal deposition unit. The 6 mm^2 pixel area measured in all cases. Thus the size of fabricated unit cells is about 6 mm^2. The final devices were encapsulated inside the inert atmosphere.

3 Results and discussions

Figure 3a shows the J–V characteristics of the fabricated devices, under illumination at AM 1.5. Table 1 summarizes the best photovoltaic characteristics, i.e., open circuit voltage (V_{oc}), short circuit current (J_{sc}), fill factor (FF), PCE, series (R_s) and shunt resistance (R_{sh}).

The PCE of devices of A, B, and C batches are 6.90%, 3.96%, and 1.60%, respectively. The batch C devices exhibited the lowest PCE as they were exposed to robust environmental impact (oxygen and water); hence its architecture (layers) gets degraded during processing and annealing. The simultaneous exposure to water and annealing decreases the device stability due to decrement of its mechanical properties. Along with that the detailed Raman study in our case highlighted that exposure to air results in structural changes in PTB7 due to air exposure. Leakage current also increases in the case when devices were fabricated in the air. For the C batch devices, the absorption intensity was also lowest in comparison to device sets A and B because of the loss of chromophores resulting from broken conjugation and chain scission due to oxidation of the PTB7 in an ambient environment. Hence, the device efficiency was lowest for the C set devices. The B sets devices exhibited intermediate PCEs as photoactive layer annealing was done in inert environment (in vacuum oven, 29 mbar), hence the mechanical properties of the active layer are less affected then type C devices. Thus, their efficiency is slightly higher than B set

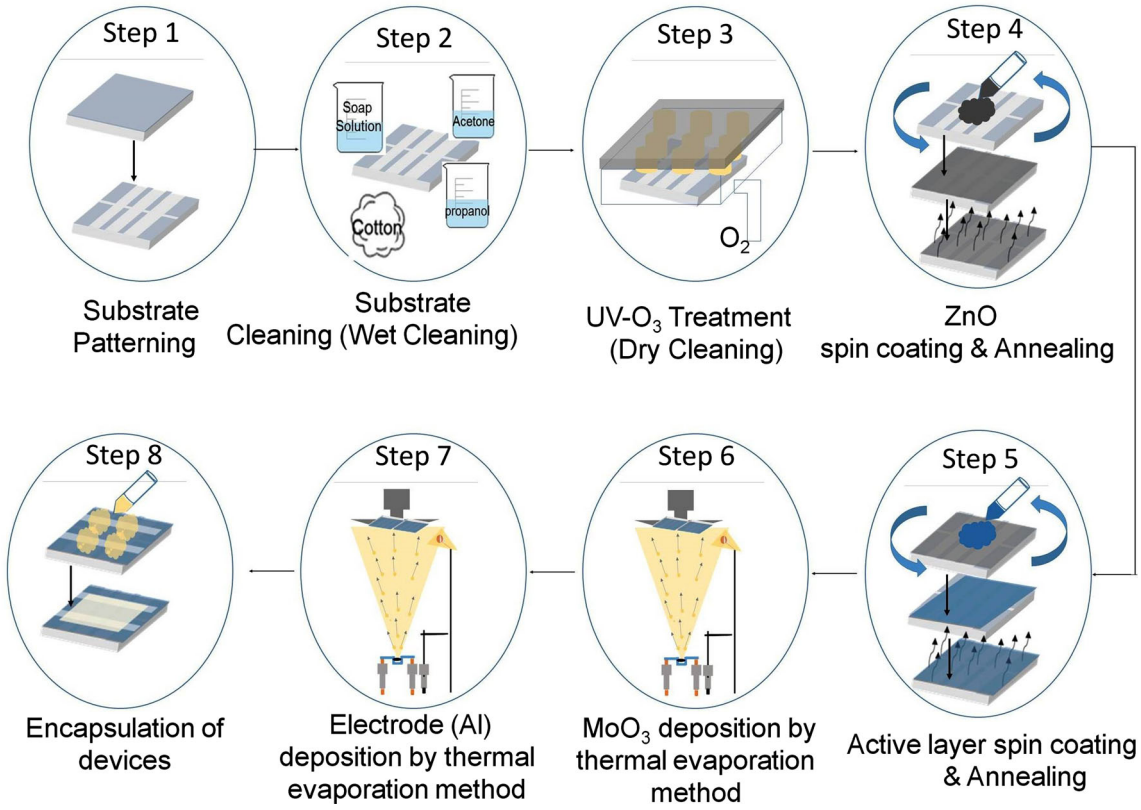

Fig. 1 Device fabrication process step by step

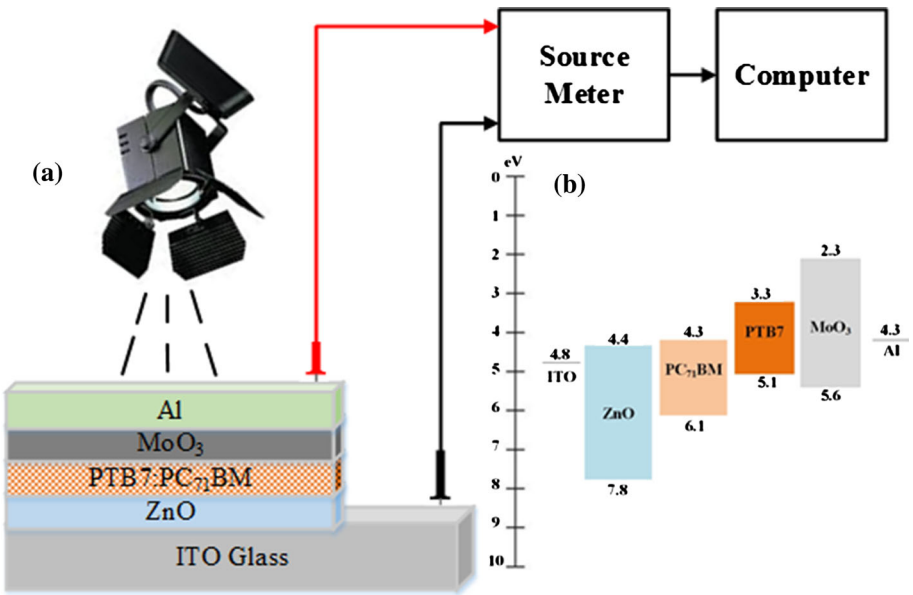

Fig. 2 **a** Device structure of fabricated solar cells, **b** energy level diagram

of devices. For the case of set A devices, the whole fabrication steps were performed inside glove box (N_2 filled), hence the degradation was minimum because of least exposure to environmental conditions (air and humidity), hence the PCE was maximum for set A devices. It is also assumed that the external stresses such as humidity affect the mechanical properties of different layers of the OPV device. It is known that exposure to humidity with simultaneous annealing results in growing of microstructures in the active layer which forms a weak layer in the bulk heterostructure of the active layer. This generated weak layer decreases the mechanical; stability of the active layer

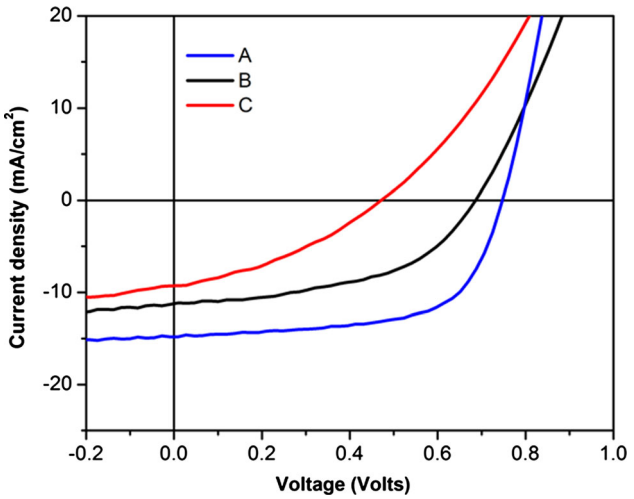

Fig. 3 **a** J–V characteristics of OSCs of A (reference device), B (annealed in vacuum), C (Annealed in ambient conditions)

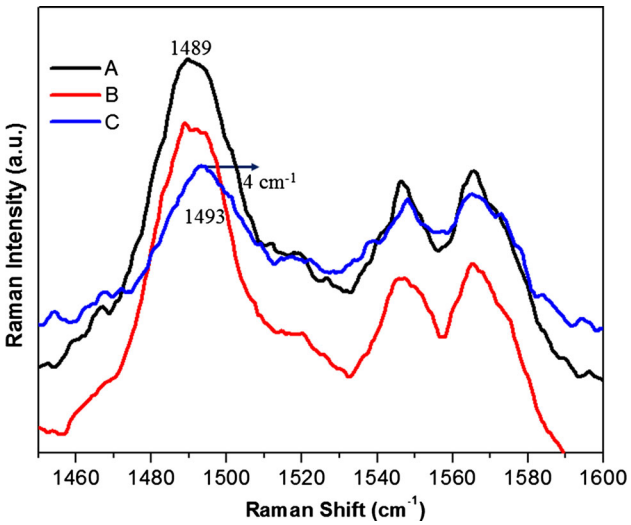

Fig. 4 Raman spectrum of fabricated OSCs of all batches

Table 1 Photovoltaic parameters of the fabricated OSCs

Devices	V_{oc} (V)	J_{sc} (mA/cm^2)	FF	PCE (%)	R_s (Ω/cm^2)	R_{sh} (kΩ/cm^2)
A	0.74	14.7	0.63	6.90	5.8	2.7
B	0.67	11.2	0.52	3.96	13	0.416
C	0.46	9.2	0.36	1.60	27.47	0.303

hence of the overall device structure (Corazza et al. 2016). Moreover, the most commonly used non-transparent electrode i.e. aluminum (Al) is reactive with water; hence it is also affected with humidity.

The parameters V_{oc}, FF, J_{sc}, and PCE of B and C batches devices were reduced in comparison to the reference devices. The batch C devices had a robust environmental impact (oxygen and water) on V_{oc}, and it gets degraded during processing and annealing. The series (R_s) and shunt (R_{sh}) resistance were calculated under light IV curve at V_{oc} and J_{sc}, respectively (Bashahu and Habyarimana 1995). The increasing value of R_s shows that the bulk resistance of active layer and the contact resistance between electrodes and layer has increased and the decreased R_{sh} witness the leakage current while handing the fabrication in the ambient conditions. The thienothiophene (TT) and benzodithiophene (BDT) alternating structure form the molecules called PTB7, which behaves as an intermolecular electron donor–acceptor system (He et al. 2014). The changes in PTB7 molecular structure under different working environment has been characterized by the Raman Spectroscopy. Figure 4 shows the Raman spectra of blend films which prepared as same as used for device fabrication. The three distinguishing peaks at 1489 cm^{-1}, 1549 cm^{-1} and 1578 cm^{-1} wavenumber observed. The Peak 1489 cm^{-1} which is corresponding to the C=C stretching mode of the BDT unit's fused thiophenes (Razzell-Hollis et al. 2014). The peak 1549 cm^{-1} and 1578 cm^{-1} corresponding to C=C stretching mode of the non-fluorinated thiophene of the TT unit, and to the C=C stretching mode of the fluorinated thiophene of TT, respectively (Razzell-Hollis et al. 2014). The peak at 1489 cm^{-1} is the main informative peak, which arises due to the conjugated backbone of PTB7. The excitation wavelength used in our case for Raman measurements is 514 nm which coincides with the absorption range of PTB7 molecules. This overlapping wavelength helps in maximizing Raman scattering from vibrational modes associated with the conjugated backbone and shows the structural changes in PTB7 due to ambient-air exposure. The calculated value of full width at half maximum (FWHM) for batch A ∼ 31.75, B ∼ 123.77, and C ∼ 219.50 at C=C stretch mode (1489 cm^{-1}) increased, which shows decreasing degree of molecular order of PTB7 chain in case of air-processing. This reduction in intensity of Raman peaks of B and C batch suggested a loss of chromophores and chains with the broken conjugated system caused due to insertion of oxygen into the film during fabrication in ambient conditions (Noh et al. 2016). Batch C, where the annealing of the photoactive layer was done in air, occurs a peak shift by 4 cm^{-1} (1489–1493 cm^{-1}), highlighting a change in bond lengths on the BDT unit after photo-oxidation (Razzell-Hollis et al. 2014). All this occurs due to the disruption of the π-conjugation.

The optical absorption spectra recorded by UV–Vis spectroscopy of films are shown in Fig. 5. The three major

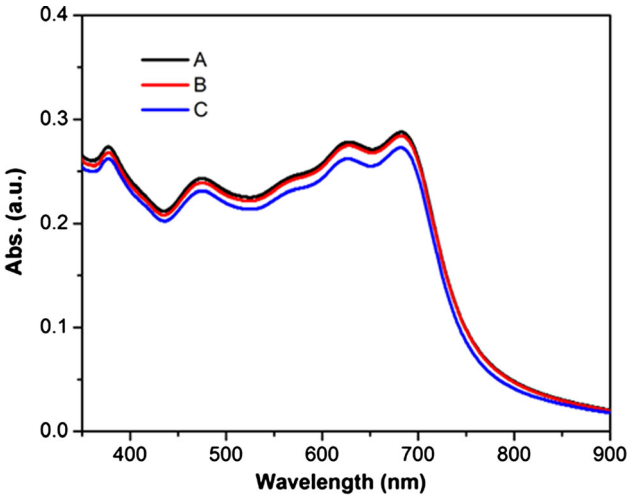

Fig. 5 Optical absorption spectra of the blended films of PTB7:$PC_{71}BM$

absorption peaks at 375 nm, 480 nm, 624 nm and 682 nm are observed in all batches film. The Where π–π* transition and internal charge transfer peaks have observed at 624 and 682 nm which demonstrating a good quality of the blend (Huang et al. 2015). Furthermore, it is witnessed that the blended films of all batches show similar behavior concerning the wavelengths. However, the intensity of absorption is different for all the cases. The enhanced absorption of light contributes to higher photocurrent generation in case A devices (Hu et al. 2013). The reason for low light absorption in case B and C is due to loss of chromophores resulting from broken conjugation and chain scission due to oxidation of the PTB7 in an ambient conditions (Razzell-Hollis et al. 2014; Alem et al. 2012).

The nanomorphology (Fig. 6) of bulk heterojunction (BHJ) films were investigated by AFM. The batch A film shows a root mean square (RMS) roughness of 4.05 nm. However, the morphology of B and C batch films shows RMS roughness of 5.55 nm and 6.67 nm, respectively. Because of the smoother morphology for devices A, the expectation of charge transport and collection are to be higher for this batch, which are in agreement with our device results (Table 1). However, the morphology of the device C is less smooth than device B. Thus, AFM results reveal that the working atmosphere and conditions have a significant effect on the morphology and roughness of the photoactive layers.

4 Conclusions

In this article, the consequence of environmental conditions on the photovoltaic performance of PTB7: $PC_{71}BM$ inverted OSCs, have been investigated. Three different sets (A, B and C) of devices were made under different processing conditions. In our case, the PCE of the solar cell devices fabricated under ambient condition (B and C) decreased by 42.62% and 431%, respectively, as compared to the reference (A) prepared in an inert atmosphere. The J–V parameters, AFM images, and the Raman spectroscopy results revealed that the annealing of the photoactive layer under vacuum has less impact on device performance compare to annealing in ambient condition. Raman spectroscopy measurement highlighted that annealing in ambient conditions leads to the insertion of oxygen into the film which influences the bond length of the electron-rich unit in PTB7 and thus causes a decrement in current and voltage values. By interpretation of the results, we have concluded that the processing environment for device fabrication contributed as an essential role in determining the output parameters of the resultant devices.

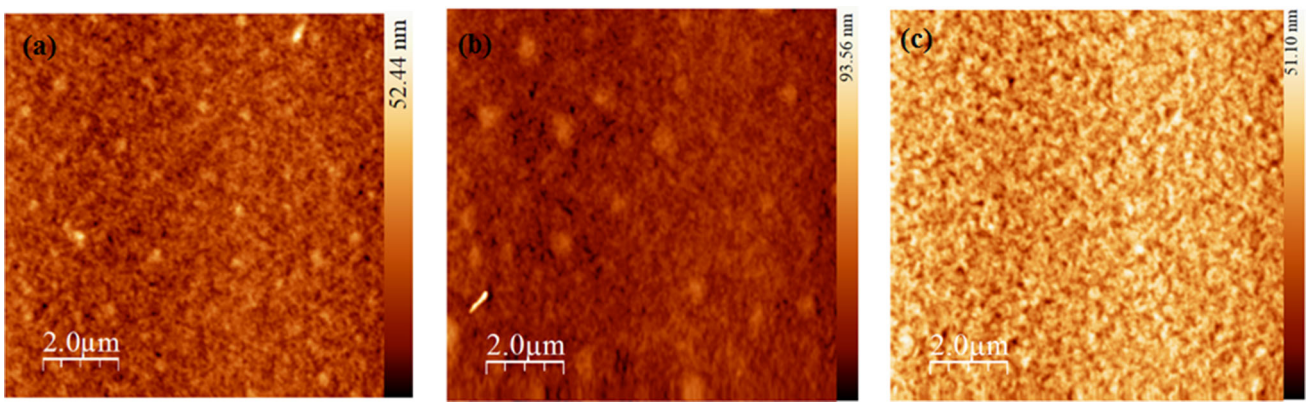

Fig. 6 AFM images of the blended films of PTB7:$PC_{71}BM$ of batch **a** A, **b** B, **c** C

Acknowledgements Author Ram Datt would like to acknowledge the financial support from UGC-SRF. We are thankful to Dr. Ritu Srivastva and Dr. Nita Dilawar for providing AFM imaging and Raman Spectroscopy facilities, respectively. Authors Sandeep Arya and Swati Bishnoi acknowledge INSA-Visiting Scientist fellowship and CSIR-RA (31/1(0494)/2018-EMR-I), respectively.

References

Alem S, Wakim S, Lu J et al (2012) Degradation mechanism of benzodithiophene-based conjugated polymers when exposed to light in air. ACS Appl Mater Interfaces 4:2993–2998. https://doi.org/10.1021/am300362b

Balderrama VS, Estrada M, Viterisi A et al (2013) Correlation between P3HT inter-chain structure and JSC of P3HT:PC[70]BM blends for solar cells. Microelectron Reliab 53:560–564. https://doi.org/10.1016/j.microrel.2012.11.006

Balderrama VS, Avila-Herrera F, Sanchez JG et al (2016) Organic solar cells toward the fabrication under air environment. IEEE J Photovolt 6:491–497. https://doi.org/10.1109/JPHOTOV.2016.2514743

Bashahu M, Habyarimana A (1995) Revew and test of method for determination of the solar cell series. Renew Energy 6:129–138

Brabec CJ (2004) Organic photovoltaics: technology and market. Sol Energy Mater Sol Cells 83:273–292. https://doi.org/10.1016/j.solmat.2004.02.030

Corazza M, Rolston N, Dauskardt RH, Beliatis M, Krebs FC, Gevorgyan SA (2016) Role of stress factors on the adhesion of interfaces in R2R fabricated organic photovoltaics Adv. Energy Mater 6:1501927

Gupta V, Lai LF, Datt R et al (2016) Dithienogermole-based solution-processed molecular solar cells with efficiency over 9%. Chem Commun 52:8596–8599. https://doi.org/10.1039/C6CC03998G

He X, Mukherjee S, Watkins S et al (2014) Influence of fluorination and molecular weight on the morphology and performance of PTB7:PC 71 BM solar cells. J Phys Chem C 118:9918–9929. https://doi.org/10.1021/jp501222w

Hu X, Wang M, Huang F et al (2013) 23% enhanced efficiency of polymer solar cells processed with 1-chloronaphthalene as the solvent additive. Synth Met 164:1–5. https://doi.org/10.1016/j.synthmet.2012.12.016

Huang D, Li Y, Xu Z et al (2015) Enhanced performance and morphological evolution of PTB7:PC 71 BM polymer solar cells by using solvent mixtures with different additives. Phys Chem Chem Phys 17:8053–8060. https://doi.org/10.1039/C4CP05826G

Noh J, Jeong S, Lee J-Y (2016) Ultrafast formation of air-processable and high-quality polymer films on an aqueous substrate. Nat Commun 7:12374. https://doi.org/10.1038/ncomms12374

Razzell-Hollis J, Wade J, Tsoi WC et al (2014) Photochemical stability of high efficiency PTB7:PC 70 BM solar cell blends. J Mater Chem A 2:20189–20195. https://doi.org/10.1039/C4TA05641H

Wang S-H, Hsiao Y-J, Fang T-H et al (2014) Effects of ITO film annealing temperature on hybrid solar cell performance. Microsyst Technol 20:1181–1185. https://doi.org/10.1007/s00542-013-1910-0

Wang J, Lu C, Higashihara T, Chen W-C (2017) All-conjugated donor–acceptor graft/block copolymers as single active components and surfactants in all-polymer solar cells. Microsyst Technol 23:1183–1189. https://doi.org/10.1007/s00542-016-3033-x

Xu X, Yu T, Bi Z et al (2018) Realizing over 13% efficiency in green-solvent-processed nonfullerene organic solar cells enabled by 1,3,4-thiadiazole-based wide-bandgap copolymers. Adv Mater 30:1703973. https://doi.org/10.1002/adma.201703973

Zhang H, Tan W-Y, Fladischer S et al (2016) Roll to roll compatible fabrication of inverted organic solar cells with a self-organized charge selective cathode interfacial layer. J Mater Chem A 4:5032–5038. https://doi.org/10.1039/C6TA00391E

Zhao W, Li S, Yao H et al (2017) Molecular optimization enables over 13% efficiency in organic solar cells. J Am Chem Soc 139:7148–7151. https://doi.org/10.1021/jacs.7b02677